ADVANCED MATERIALS TECHNOLOGIES
www.advmattechnol.de

Hollow-Micropillared Glass Fabricated on Hollow Joe Pye Weed-Inspired Tubes for Detecting Molecular Signatures

*Anastasia L. Novikova, Aviad Katiyi, Uzziel Sheintop, Meng Zhang, Pengfei Wang, and Alina Karabchevsky**

A rational design and fabrication approach is proposed for suspended multicore fibers, resulting in the creation of dual-core and triple-core suspended fibers with different diameters and one-side cladding. These fibers are tailored for near-infrared spectroscopy applications. The multicore-suspended fibers offer an amplified electromagnetic field effect due to the exposure of the core to the analyte, leading to a significant 16 *dB* drop in transmittance at the fingerprint absorption line of the analyte. Numerical models indicate that the suspended core with a diameter of 3.52 µm exhibits a superior evanescent field in the boundary between the core and the contact point with the cladding, in comparison to the tested cores with diameters of 3.99 and 12.06 µm. The successful fabrication of these multicore-suspended fibers represents a promising advancement toward achieving highly sensitive molecular signature detection capabilities.

1. Introduction

In the past few years, the global community has faced the pressing challenge of declining air, soil, and water quality. The root cause of these issues can be traced back to human activities, notably industrial operations,[1] transportation, domestic pollution, and the environmental disasters resulting from these issues.[2] The main pollutants in water are heavy metals, radioactive elements, oil products, biogenic elements, medical-biological elements, and microplastics.[3–5] Air pollution primarily consists of heavy metals, CO_2, sulfur dioxide, nitrogen, slurry, and methane, serving as the main pollutants.[6,7] These pollutants have the potential to induce a range of health issues affecting the vascular, respiratory, circulatory, central, and peripheral nervous systems. To identify the presence of these substances in air and water, diverse techniques are available, including physical, chemical, and mechanical tests. Nevertheless, not all of these methods are suitable for detecting the wide array of substances that may act as pollutants in air or water. Moreover, their inability to provide real-time sensing poses a limitation. To address intricate pollution challenges effectively, spectroscopic methods offer a viable solution.[8–14] The common spectroscopic methods are presented in **Table 1**.

Molecular absorption spectroscopy stands out as one of the most efficient approaches for pollutant sensing. Widely adopted and esteemed in the field of spectroscopy, this technique comprises a group of methods unified by the core principle of measuring the absorption of radiation by a sample as a function of frequency or wavelength. As the radiation traverses the sample, its molecules selectively absorb photons, resulting in an absorption band, which serves as a unique fingerprint of the sample. The versatility of absorption spectroscopy allows for measurements across the entire electromagnetic spectrum, enabling the examination of multiple pollutants of diverse types. Moreover, this method accommodates the analysis of substances in various states of aggregation, thereby offering valuable insights into the chemical nature of the substance under investigation.[38,39]

Optical guided wave structures, such as optical fibers and waveguides, offer promising platforms for molecular spectroscopy. Among these, optical fibers have emerged as prominent tools for detecting low-concentration substances in both air and water, owing to their user-friendly nature and compact dimensions.[40–42] A wide range of fiber configurations and compositions are available, providing researchers with the flexibility to cater to specific research objectives and analyze diverse materials and their individual concentrations effectively.[43–45] For instance, tapering commercial optical fibers to microfiber enables the attainment of high sensitivity, making them valuable for applications as chemical and biological sensors.[12,46] However, in scenarios where research is conducted in natural environments or hazardous settings, the demand for compact and robust sensing devices becomes crucial.

A. L. Novikova, A. Katiyi, U. Sheintop, A. Karabchevsky
School of Electrical and Computer Engineering
Ben-Gurion University of the Negev
David Ben Gurion Blvd. 1, Beer-Sheva 8410501, Israel
E-mail: alinak@bgu.ac.il

M. Zhang, P. Wang
Key Laboratory of In-Fiber Integrated Optics of Ministry of Education
College of Physics and Optoelectronic Engineering
Harbin Engineering University
Harbin 150001, China

The ORCID identification number(s) for the author(s) of this article can be found under https://doi.org/10.1002/admt.202301245

DOI: 10.1002/admt.202301245

Table 1. Spectroscopic methods for determining substances in air and water.

Method	Pollutions	Applications	Ref
Molecular absorption spectroscopy	O_2, CO_2, H_2O, HCl, NH_3, NO_x heavy metals, CO_2, sulfur dioxide,	industrial pollution, breath analysis soil, analysis and control of chemical reactions, atmosphere, water	[9,15–18]
Nephelometric and turbidimetric spectroscopy	viruses, cells, low molecular weight compounds, amino acids, proteins, macromolecules, bacteria	Biological fluids, water	[19–23]
Luminescent analysis	Organic pollutants, heavy metals, inorganic pollutant, bio objects	food quality control, biological monitoring, chemical threat detection, and chemical sensing for environmental analysis	[24–28]
Magnetic resonance spectroscopy	viruses, bacteria, cells, bio object	living tissues, fluids	[29–32]
X-ray spectroscopy	Organic pollutants, heavy metals, inorganic pollutant, bio objects	environmental, chemical and biological monitoring	[33–37]

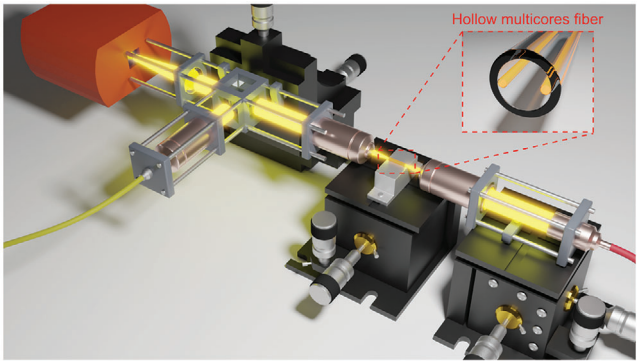

Figure 1. Illustration of the experimental setup of multi-core fiber sensor. The inset shows a zoom-in of the hollow-core fiber.

A promising optical fiber configuration that holds great potential for sensing applications is the use of multi-core suspended fibers. Hollow multi-core fibers have the advantage of operating within liquid or gas volumes, amplifying signals through multiple cores without requiring size or surface modifications. These fibers incorporate several cores within a single fiber cladding, enabling parallel transmission paths through distinct spatial cores in a single fiber, thereby significantly enhancing sensitivity. While the number of cores in a multi-core fiber is limited to avoid potential interactions between them, various structural solutions are implemented to address this limitation. For instance, employing cores with identical parameters allows for simultaneous signal transmission. Each core within the multi-core fiber behaves like a conventional single-mode fiber, supporting various information transmission technologies. As a result, multi-core fibers find application in diverse fields, including sensing,[47–51] telecommunication,[52–55] and laser technologies.[56–59]

Here, we report the design, fabrication, and proof-of-concept demonstrations of dual-core and triple-core (type I and type II) suspended hollow fibers for absorption spectroscopy, as depicted in **Figure 1**. These environmentally safe fibers enable real-time operation and user-friendly detection of chemical, medical, and biological entities. The inspiration for developing such multi-core fibers stems from the plant named Eutrochium fistulosum, commonly known as Hollow Joe Pye Weed.[60,61] The plant's hollow stem is naturally lined with fibers that serve a sealing function. However, in nature, these fibers remain confined within the plant tissues and do not connect with other fibers. In our research, we harnessed the concept of multi-core fibers to identify the absorption of N-methylaniline ($C_6H_5NH(CH_3)$) in a hexane mixture. N-methylaniline is a highly toxic substance classified under hazard class 2.[62,63] Our findings indicate that both type I and type II triple-core fibers demonstrate high sensitivity to gases. Through numerical simulations, all fiber types exhibited remarkable sensitivity in detecting N-methylaniline at a concentration ratio of 1:3 to hexane. Notably, triple-core fiber type I with test strands demonstrated the highest sensitivity among all configurations.

2. Results and Discussion

2.1. Numerical Simulation

To understand the interaction of light with molecules in multi-core suspended fibers, we performed a numerical simulation using Lumerical MODE, when the medium around a core corresponds to the complex refractive index of N-Methylaniline. Specifically, we studied the excitation modes in hollow multi-core fibers at a wavelength of 1.5 μm, which corresponds to the absorption of the first overtone of the N-H bond of N-methylaniline.[11] **Figure 2** shows the numerical simulation results for three different multi-core suspended fibers architectures: dual-core, triple-core type I, and triple-core type II in air. The dual-core fibers are suspended fibers with two equidistant cores of 12.06 μm in diameter, a hole diameter of 85.56 μm, a cladding diameter of 127.94 μm and confinement factor of $\Gamma = 0$. The triple-core fiber type I is a hollow fiber with three equidistant cores of diameters of 3.99 μm, an air hole diameter of 76.84 μm, a cladding diameter of 128.96 μm, and $\Gamma = 0$. The triple-core suspended fiber type

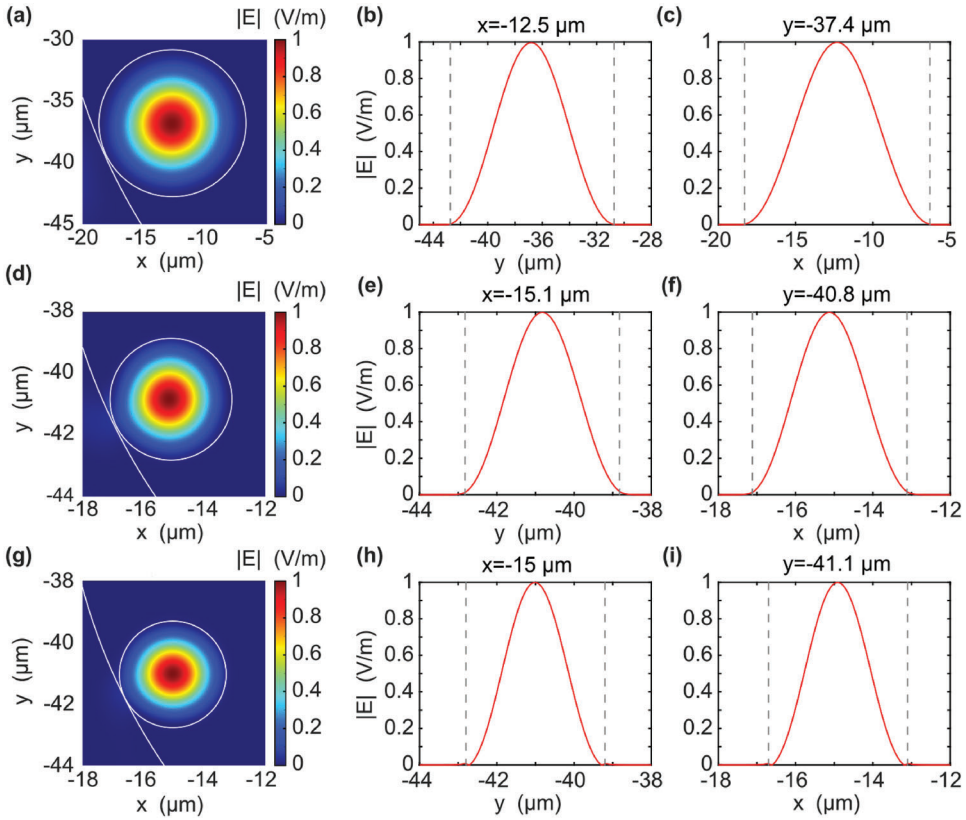

Figure 2. Calculated electric field at a wavelength of 1.5 μm for three types of multi-core fibers, a) dual-core, d) triple-core type I, and g) triple-core type II, in air - and the cross-sections at $x = 0$ (b, e, h) and $y = 0$ (c, f, i) are shown in columns, respectively.

II has three equidistant cores of 3.52 μm, an air hole diameter of 93.43 μm, a cladding diameter of 123.52 μm, and $\Gamma = 0$. We can see that for all types of fibers, $\Gamma = 0$, which means that the diameter of the cores is large.

Figure 3 shows the results of numerical simulations for three fiber designs of dual-core, triple-core type I, and triple-core type II, in a mixture of N-methylaniline in hexane[11] - for the same parameters of the fiber described above. The considered wavelength is 1.496 μm, and the refractive index of N-methylaniline in hexene mixture is $n = 1.429$. One can see, from the subplots in Figure 3d,g, a large evanescent field in the medium, extending beyond the fiber core. From the calculations of the confinement factor, we learn that the values of Γ are as follows: for dual-core $\Gamma = 0.1136$, for triple-core type I $\Gamma = 0.0338$, and for triple-core type II $\Gamma = 0.0201$.

2.2. Fibers Composition

Figure 4a-c shows images of hollow multi-core fibers for dual-core fiber, triple-core, fiber type I and triple-core fiber type II, respectively. We investigated the composition of the fibers using a scanning electron microscope (SEM). Figure 4e-g shows the scanning electron micrographs of the hollow multi-core fibers surfaces.

The fibers were placed perpendicular to the stage so that the cores were imaged (from left to right triple-core fiber type I, dual-core fiber, triple-core fiber type II), as shown in Figure 4d. Figure 4e shows part of the triple-core fiber type I with cladding and one core. It can be seen that it is in slight contact with the cladding, and a small illumination is visible on the surface. This indicates that there are several substances on the surface of the core, which were studied using energy-dispersive X-ray spectroscopy (EDS). Figure 4f shows the dual-core fiber. The location of the cores is clearly visible, and the cores are parallel and equidistant from each other. Figure 4g shows part of a triple-core fiber type II with one core. The cores are also equidistant from each other.

Next, the elemental composition of the fibers was determined using EDS. For this, we conducted elemental composition studies for dual-core fiber. The data for dual-core hollow fiber are presented in **Table 2**.

We examined two areas in the fiber - the surface of the fiber and its core. Table 2 shows that two-core hollow fibers are composed of SiO_2 dopped with 3.5% germanium. The concentration of oxygen is 32.525% and silicon 63.925%. The cladding has an oxygen concentration of 32.21% and silicon 67.78%. The main part of the fiber is silicon.

Next, we perform a compositional study for the triple-core fiber type I. The data are presented in **Table 3**.

In our investigation, we focused on two regions within the fiber: the cladding and the core. Table 3 provides the composition details of the triple-core hollow fibers type I, which are composed of SiO_2 with 3.025% germanium. The core contains

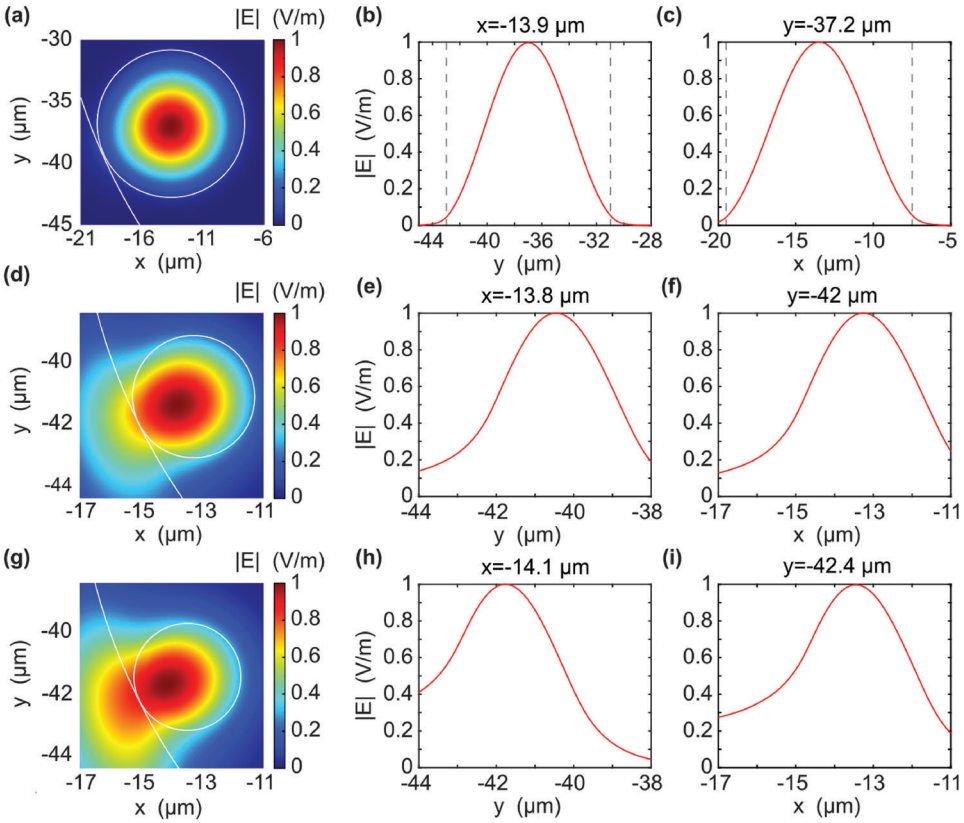

Figure 3. Calculated electric fields (normalized to the maximum) at a wavelength of 1.496 μm for three types of multi-core fibers, a) dual-core, d) triple-core type I, and g) triple-core type II, in a mixture of N-methylaniline in hexane 1:3. Respective cross-sections at $x = 0$ (b, e, h) and $y = 0$ (c, f, i) are shown in columns.

Table 2. Elemental composition of dual-core fiber.

Core			Cladding		
Element	Atomic concentration [%]	Weight concentration [%]	Element	Atomic concentration [%]	Weight concentration [%]
O	32.525	20.220	O	32.211	21.300
Si	63.925	69.770	Si	67.789	78.700
Ge	3.549	10.010			

a higher concentration of oxygen (67.15%) and silicon (29.825%) compared to the dual-core fiber. In contrast, the cladding comprises 39.70% oxygen and 60.63% silicon. This disparity in oxygen content between the core and cladding is observed in the triple-core fiber configuration.

The composition of a triple-core fiber of type II is shown in **Table 4**.

In our study, we investigated two specific regions: the cladding and the core. Table 4 outlines the composition of the triple-core hollow fibers of type II, which consist of SiO_2 with an additional 2.8% germanium, a lower percentage compared to the previous fibers. The core exhibits a higher concentration of oxygen (67.567%) and silicon (31.613%) relative to the dual-core fiber. However, the ratio of oxygen content in the core compared to the cladding is similar to that of the triple-core type I fiber. Meanwhile, the cladding contains 55.973% oxygen and 44.027% silicon.

2.3. Experimental Results

To test the suspended fibers in a molecular medium, we constructed the experimental setup illustrated in **Figure 5**a. Initially, a broadband laser source was coupled into a single-mode fiber using an objective lens. The coupling was optimized to achieve the best signal output, and the single-mode fiber was then connected to an optical spectrum analyzer for signal measurement. Subsequently, a silver reflective collimator was used to collimate the beam from the fiber, which was directed back to the fibers through a long working distance objective with a magnification of ×100. The sensing multi-core fiber was positioned on a Teflon

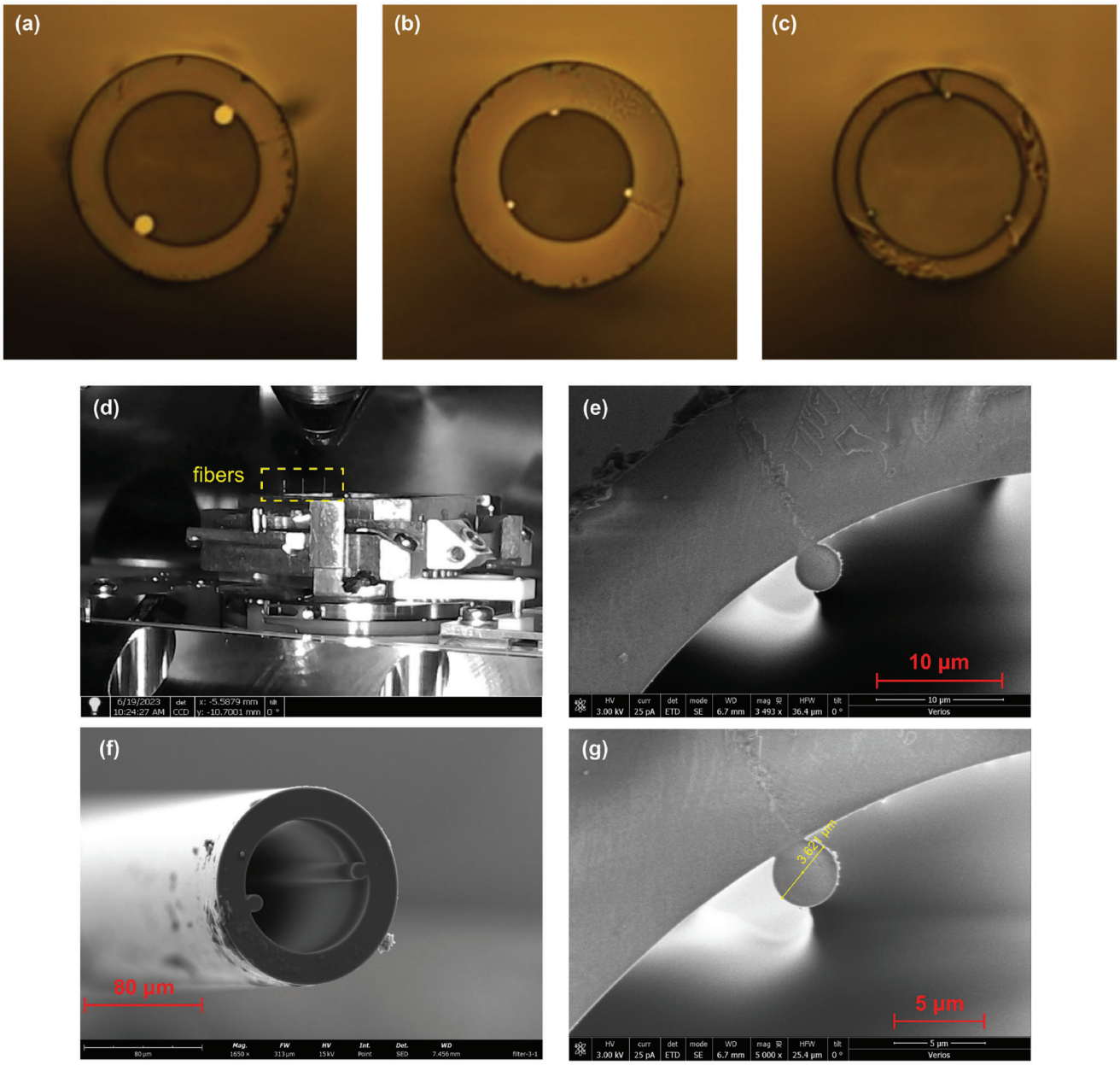

Figure 4. Images of hollow multi-core fibers for a) dual-core fiber, b) triple-core fiber type I and c) triple-core fiber type II. Scanning electron micrographs (SEM): d) A photograph of hollow multi-core fibers in SEM setup with a dashed box surrounding fiber fixed in the holder. e) Zoomed-in image of triple-core fiber type I. f) Dual-core fiber. g) Zoomed-in image of triple-core fiber type II.

Table 3. Elemental composition of triple-core fiber type I.

Core			Cladding		
Element	Atomic concentration [%]	Weight concentration [%]	Element	Atomic concentration [%]	Weight concentration [%]
O	67.150	50.400	O	39.370	27.000
Si	29.825	39.300	Si	60.630	73.000
Ge	3.025	10.300			

Table 4. Elemental composition of triple-core fiber type II.

Core			Cladding		
Element	Atomic concentration [%]	Weight concentration [%]	Element	Atomic concentration [%]	Weight concentration [%]
O	67.567	49.000	O	55.973	42.000
Si	31.631	41.500	Si	44.027	58.000
Ge	2.802	9.500			

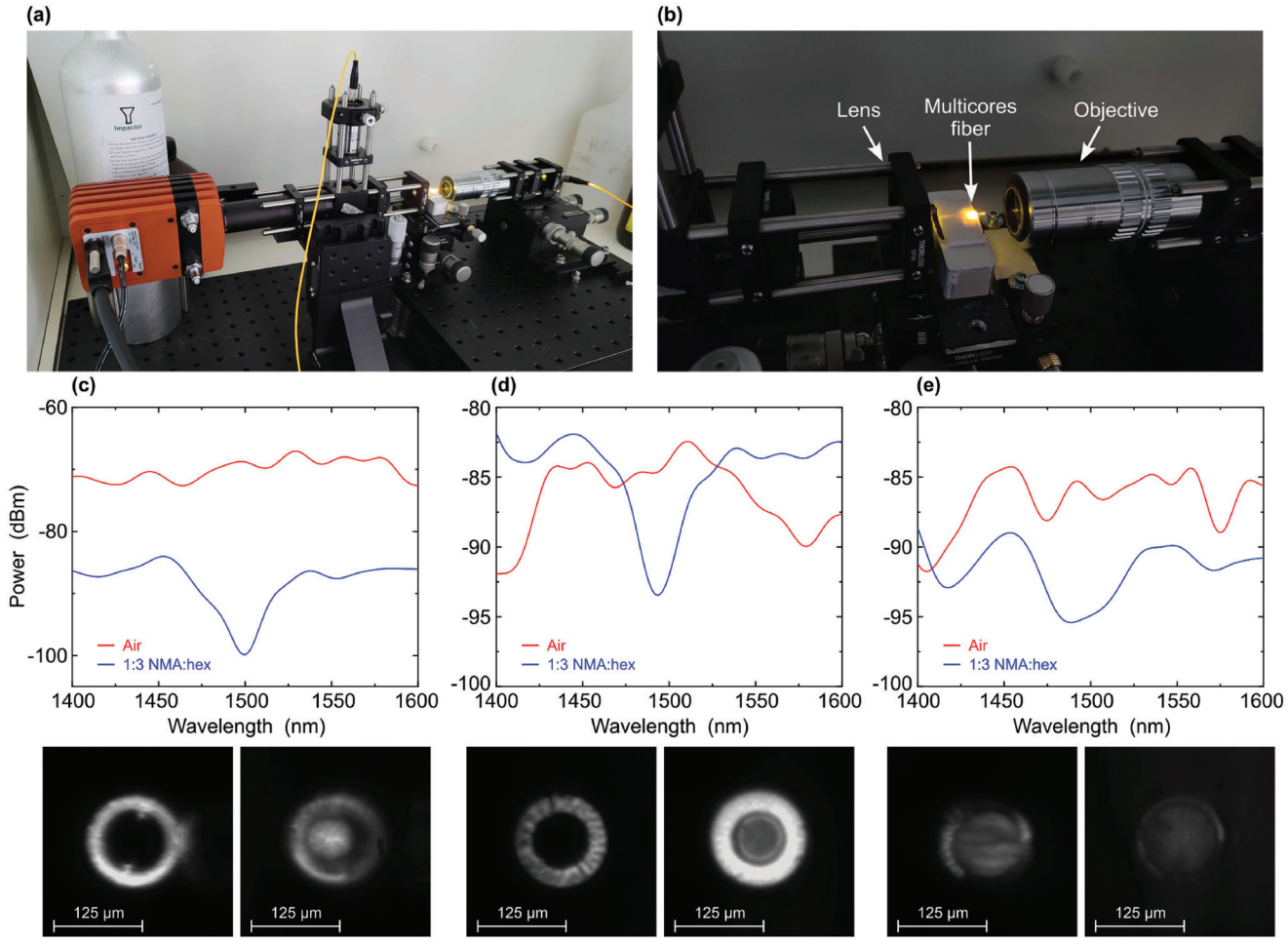

Figure 5. a) Experimental setup constructed for the hollow multi-core fibers experiment. b) Zoom in on the fiber sensing structure with the sample on the Teflon spacer. Measured transmittance spectra in air (red curve) and in a mixture of N-methylaniline in hexane (blue curve) with a concentration of 1:3 (NMA/hexane) at wavelength range of 1.4–1.6 µm for c) dual-core fiber, d) triple-core fiber type I and e) triple-core fiber type II. The photos of the output for clean (left) and NMA with hexane mixture (right) are shown under the graphs.

spacer placed on a three-axis linear stage with two-axis rotation, situated between the coupling and collection setups, as depicted in Figure 5b.

For signal collection, an aspheric lens was utilized to gather the output of the fiber. The output signal was divided into two parts by a beam splitter: the first part was directed to a camera for facet and mode imaging studies. Once the setup was aligned, the signal was collected using a spectrum analyzer. The spectrum was measured within a wavelength range of 1400–1600 nm, suitable for capturing the absorption of the first overtone of the N-H bond of N-methylaniline (NMA) at 1.496 µm.[64] The study involved investigating a mixture of N-methylaniline in hexane with a concentration ratio of 1:3 (NMA:hexane). This mixture possesses a refractive index of 1.429, enabling efficient guiding in the silica ($n = 1.445$) core of the multi-core fibers under examination.

To obtain a reference spectrum, we measured the transmission of fibers in air. Next, we measured the transmission of the fibers with the N-methylaniline in hexane mixture. The fibers were im-

mersed in a solution of N-methylaniline with hexane for 30 min, and placed back on the Teflon spacer. The experimental results for the three types of fibers are shown in Figure 5c-e.

Figure 5c shows measurements of a clean dual-core fiber with N-methylaniline with hexane in the near-IR ranges of 1400–1600 nm. The N-methylaniline absorption is shown at 1500 nm with a value of 12 dBm. Figure 5d shows measurements of a clean triple-core fiber type I with N-methylaniline with hexane. The N-methylaniline absorption is shown at 1496 nm with 16 dBm. The dip is sharper and the peak shoulder smaller, compared to triple-core fibers. We can also see that, upon application of liquid, the signal from the fiber itself gets stronger. Figure 5e shows measurements of a clean triple-core fiber type II; and with N-methylaniline with hexane. The absorption of N-methylaniline, as well as other types of fibers, is shown at 1496 nm with a value of 6 dBm. Its dip is wider, and the shoulder of the peak is longer than the rest of the dual-core and triple-core type I fibers.

In conjunction with the spectral measurements, we conducted investigations on the intensity distributions of the modes throughout the entire fiber using a VIS-SWIR camera. The results are presented in Figure 5. Figure 5c (bottom) displays the field intensity distributions at the output facet of the dual-core fiber, both before and after the addition of NMA. In the absence of NMA, the cores and cladding are clearly visible in the mode of the dual-core fiber. However, upon introducing NMA, only the cladding is visible due to the presence of the liquid being studied inside the fiber. As the liquid dries, the core reappears.

Similarly, Figure 5d (bottom) depicts the intensity distributions for a triple-core fiber type I, before and after the addition of NMA. Without NMA, the cores are not visible, but the cladding ring is distinctly expressed in the mode of the triple-core fiber type I. Upon adding NMA, both the cladding and some portions of the core become visible. Notably, there is an increase in the visibility of the mode, as confirmed by experimental observations.

Furthermore, Figure 5e (bottom) exhibits the output of a triple-core fiber type II before and after the addition of NMA. In the absence of NMA, the cores are not visible due to their smaller diameter compared to a dual-core fiber, leaving only the cladding visible. However, when the liquid is present in the fiber, the visibility of the cladding is reduced, similar to the effect observed in the dual-core fiber configuration.

3. Conclusion

In conclusion, our research involved the fabrication and comprehensive testing of various types of hollow multi-core fibers for detecting substances and their concentrations in air and water, employing both numerical simulations and experimental investigations. The results revealed that triple-core fibers of type I and type II exhibited the highest sensitivity when compared to dual-core fibers, making them promising candidates for detecting gases and pollutants in the air, especially considering the similar refractive indices of gases.

For the identification of N-methylaniline absorption with a concentration of 1:3 to hexane, all types of fibers showed high sensitivity in numerical simulations. However, in practical experiments, the triple-core fiber type I demonstrated the highest sensitivity, manifesting a smoother, improved signal with a larger peak compared to other fiber types. The unique advantages of this type of fiber include its mechanical stability, composition of environmentally friendly silicon oxide allowing easy recycling, extended operational capability, immediate signal reception, and the potential for increased peak intensity as the sample dries within the fiber.

Hollow multi-core fibers with various core configurations hold significant potential for diverse applications in different industries. They can facilitate substance detection and monitoring in environmental protection efforts, encompassing water, soil, and air pollution control. Additionally, these fibers find utility in medicine for detecting viruses, bacteria, cells, low molecular weight compounds, amino acids, proteins, and macromolecules. Pharmacology can benefit from these fibers by studying new substances, ensuring product quality, and determining concentrations of essential drugs in preparations. Moreover, their deployment in hazardous industries and disaster areas allows for the precise determination of low concentrations of substances, aiding in safety measures and response strategies.

4. Experimental Section

Materials: Hexane (C_6H_{14}, ⩾95%) and N-methylaniline ($C_6H_5NH(CH_3)$, ⩾98%) were purchased from Sigma–Aldrich.

Fabrication of the Hollow Multi-Core Fiber: The fabrication technology of the embedded core hollow fiber included two steps: preform preparation and fiber drawing, as the traditional commercial optical fiber. The core fiber preform was fabricated by using a modified "suspended core-in-tube technique". First, the core rod was manufactured by modified-chemical-vapor-deposition (MCVD) and etching method and then inserted into the silica tube placed horizontally. As a result, the core rod would be parallel with the silica tube axially because of the core rod gravity. Next, in order to make the core rod more tightly fixed on the inwall of the silica tube, the core rod and the tube were moved horizontally and heated by an oxy-hydrogen torch and then melted together for a period of time. Finally, the preform was tapered in one end to form a cone shape to avoid introducing carbon dust or other impurities into the silica tube during the fiber drawing process. The silica tube became the cladding when the assembled preform was drawn into fiber. For a fiber drawing tower, to avoid collapsing the silica tube at a higher drawing temperature, it was necessary to attach a pressure controller to provide positive pressure. During the fiber drawing process, the air pressure in the silica tube and the drawing temperature were both important for controlling the shape and size of the suspended core. After a series of experiment parameters tests, it successfully prepared tens of meters of suspended dual-core and triple-core hollow fiber, respectively as shown in Figures 4 and 5.

Fabrication of the Sensing Device: Dual-core and triple-core (type I and type II) suspended fibers were used as sensing devices. In the first stage, it cut off 6 cm of each fiber and removed the polymer coating by placing the fiber in acetone for 1 h and drying under a temperature of 25°C. Then, 2 cm were cut from the clean fibers and the fibers were attached to a Teflon slide with transparent double-sided tape.

Obtaining Composite Materials: To obtain N-methylaniline suitable for research in fiber, it mixed N-methylaniline with hexane in glass flasks with a capacity of 5 ml in proportions of 1 to 3, where 1 was the number of portions of N-methylaniline, 3 was the proportion of hexane and 1 portion was 200 µl. The solutions were stored at room temperature in a laminar flow device.

Application of the Composite Material to the Surface of the Fiber: 2 cm of the fiber were cut from the cleaned fibers and placed in a solution of N-methylaniline with hexane for 30 min. The samples were removed from the solutions, and dried at a temperature of 25°C for 10 min, and the fibers were attached to a Teflon glass slide using transparent double-sided adhesive tape.

Experiment Optical Set-Up: A broadband laser source (Fianium WL-SC-400-8-PP), with a wavelength range from 400 to 2400 nm, was coupled into a single mode fiber using Olympus plan achromat objective with NA 0.25 and magnification ×10. The fiber was connected to a silver reflective collimator with a beam diameter of 2 mm, creating a collimated beam. The collimated beam was focused on the fiber input facet using a long working distance microscope objective with a magnification of ×100, a numerical aperture of 0.55 and a working distance of 13 mm. The input coupling setup was aligned to the fiber using a three-axis stage (three-Axis NanoMax Stage). The fiber was placed on a Teflon spacer using double-sided tape. The Teflon spacer was placed on a three-axis stage (MicroBlock MBT616D) with a two-axis rotation stage for a precise angle alignment. The output collection setup was built using a cage system for verifying an alignment with accurate angles between the optical components. The output beam was collected using an aspheric lens with a focal distance of 11 mm. The beam was split using a beam splitter. Half of the beam was focused with a lens on a VIS-SWIR camera (Ninox-640) for monitoring the output beam to verify a precise alignment for both input and output. The second half of the output beam was coupled into a single mode fiber using Olympus plan achromat objective with NA 0.25 and magnification ×10. The output collection setup was placed on a three-axis stage. The fiber was connected to an optical spectrum analyzer (Yokogawa 6370D) with a resolution of 2 nm.

Signal Smoothing: To improve the quality of the data by reducing the noise, a Butterworth filter was applied using Python for smoothing the signals. By applying the Butterworth filter to the sample, the noise was effectively smoothed, resulting in a cleaner and more reliable representation of the transmission. This was achieved by minimizing both the ripple in the passband and the transition bandwidth.

Acknowledgements

The filtering method utilized by Alex Dobrovolsky and Eyal Rozenwald. The research reported in the paper was funded by the European Union's Horizon 2020 research and the innovation program under the Marie Skłodowska-Curie grant agreement No. 872662 and the Israel Science Foundation (ISF) grant No. 2598/20.

Conflict of Interest

The authors declare no conflict of interest.

Data Availability Statement

The data that support the findings of this study are available from the corresponding author upon reasonable request.

Keywords

dual core fiber, spectroscopy, suspended waveguides, triple core fiber

Received: July 27, 2023
Revised: November 5, 2023
Published online:

[1] M. Saidova, A. Yadgarov, D. Kodirova, J. Turdialiev, G. Embergenova, in *E3S Web of Conferences*, vol. *377*, EDP Sciences, Les Ulis **2023**, p. 03017.
[2] C. M. How, Y.-H. Kuo, M.-L. Huang, V. H.-C. Liao, *Sci. Total Environ.* **2023**, *858*, 159732.
[3] C. H. Walker, *Organic pollutants: an ecotoxicological perspective*, CRC press, Boca Raton **2008**.
[4] V. Wankhade Atul, G. Gaikwad, M. Dhonde, N. Khaty, S. Thakare, *Res. J. Chem. Environ* **2013**, *17*, 84.
[5] Y. Tang, Y. Liu, Y. Chen, W. Zhang, J. Zhao, S. He, C. Yang, T. Zhang, C. Tang, C. Zhang, Z. Yang, *Sci. Total Environ.* **2021**, *766*, 142572.
[6] A. Talaiekhozani, S. Rezania, K.-H. Kim, R. Sanaye, A. M. Amani, *J. Cleaner Prod.* **2021**, *278*, 123895.
[7] C. Bogdal, M. Scheringer, E. Abad, M. Abalos, B. Van Bavel, J. Hagberg, H. Fiedler, *TrAC, Trends Anal. Chem.* **2013**, *46*, 150.
[8] A. Karabchevsky, A. Kavokin, *Sci. Rep.* **2016**, *6*, 1.
[9] A. Karabchevsky, A. Katiyi, A. S. Ang, A. Hazan, *Nanophotonics* **2020**, *9*, 3733.
[10] A. Karabchevsky, U. Sheintop, A. Katiyi, *ACS Sensors* **2022**, *7*, 2797.
[11] A. Katiyi, A. Karabchevsky, *J. Lightwave Technol.* **2017**, *35*, 2902.
[12] A. Katiyi, J. Zorea, A. Halstuch, M. Elkabets, A. Karabchevsky, *Biosens. Bioelectron.* **2020**, *161*, 112240.
[13] C. Pasquini, *Anal. Chim. Acta* **2018**, *1026*, 8.
[14] O. Borovkova, D. Ignatyeva, S. Sekatskii, A. Karabchevsky, V. Belotelov, *Photonics Res.* **2020**, *8*, 57.
[15] M. A. Abdelaziz, M. Shaldam, R. A. El-Domany, F. Belal, *Spectrochim. Acta, Part A* **2022**, *264*, 120298.
[16] F. Huth, A. Govyadinov, S. Amarie, W. Nuansing, F. Keilmann, R. Hillenbrand, *Nano Lett.* **2012**, *12*, 3973.
[17] F. M. Hoffmann, *Surf. Sci. Rep.* **1983**, *3*, 107.
[18] K. Laqua, W. Melhuish, M. Zander, *Pure Appl. Chem.* **1988**, *60*, 1449.
[19] C. Price, K. Spencer, J. Whicher, *Ann. Clin. Biochem.* **1983**, *20*, 1.
[20] M. Infantino, B. Palterer, S. Pancani, M. Benucci, V. Grossi, M. Manfredi, N. Bizzaro, *Clin. Chem. Lab. Med. (CCLM)* **2023**, *61*, 1619.
[21] K. M. Lao, A. Pokharel, M. M. M. I. Elzieny, E. Sykes, S. M. Truscott, *Lab. Med.* **2023**, lmad043.
[22] M. Imoto, T. Kamisako, K. Watanabe, T. Yamada, *Clin. Lab.* **2022**, *68*, 12.
[23] N. Rollborn, J. Jakobsson, A. Campbell, G. Nordin, M. Karlsson, A. Larsson, K. Kultima, *Clin. Biochem.* **2023**, *111*, 47.
[24] L. Shi, N. Li, D. Wang, M. Fan, S. Zhang, Z. Gong, *TrAC, Trends Anal. Chem.* **2021**, *134*, 116131.
[25] I. Costas-Mora, V. Romero, I. Lavilla, C. Bendicho, *TrAC, Trends Anal. Chem.* **2014**, *57*, 64.
[26] J.-C. G. Bünzli, C. Piguet, *Chem. Soc. Rev.* **2005**, *34*, 1048.
[27] W. R. Baeyens, *Luminescence techniques in chemical and biochemical analysis*, vol. *12*, CRC Press, Boca Raton **1990**.
[28] Y. Zhong, J. Gu, Y. Su, L. Zhao, Y. Zhou, J. Peng, *Chem. Eng. J.* **2022**, *433*, 133263.
[29] T. Nakahara, S. Tsugawa, Y. Noda, F. Ueno, S. Honda, M. Kinjo, H. Segawa, N. Hondo, Y. Mori, H. Watanabe, K. Nakahara, K. Yoshida, M. Wada, R. Tarumi, Y. Iwata, E. Plitman, S. Moriguchi, C. de la Fuente-Sandoval, H. Uchida, M. Mimura, A. Graff-Guerrero, S. Nakajima, *Mol. Psychiatry* **2022**, *27*, 744.
[30] A. Rietzler, R. Steiger, S. Mangesius, L.-M. Walchhofer, R. M. Gothe, M. Schocke, E. R. Gizewski, A. E. Grams, *J. Neuroradiol.* **2022**, *49*, 370.
[31] B. Bakhritdinov, M. Aliev, G. Mardieva, *World Bulletin of Public Health* **2022**, *8*, 149.
[32] J. Snyder, D. Noujaim, T. Mikkelsen, in *Handbook of Neuro-Oncology Neuroimaging*, Elsevier, Amsterdam **2022**, pp. 385–394.
[33] B. K. Agarwal, *X-ray spectroscopy: an introduction*, vol. *15*, Springer, Berlin **2013**.
[34] F. De Groot, *Coord. Chem. Rev.* **2005**, *249*, 31.
[35] C. Bonnelle, *Annu. Rep. Sect. "C" (Phys. Chem.)* **1987**, *84*, 201.
[36] J.-J. Velasco-Vélez, J. Poon, D. Gao, C.-H. Chuang, A. Bergmann, T. E. Jones, S.-C. Haw, J.-M. Chen, E. Carbonio, R. V. Mom, et al., *Adv. Sustainable Syst.* **2023**, 2200453.
[37] J. Staunton, F. Paerels, *The Astrophysical J.* **2023**, *949*, 26.
[38] M. H. Penner, *Food Anal.* **2017**, 79.

[39] R. Berera, R. van Grondelle, J. T. Kennis, *Photosynth. Res.* **2009**, *101*, 105.
[40] F. Chiavaioli, P. Zubiate, I. Del Villar, C. R. Zamarreño, A. Giannetti, S. Tombelli, C. Trono, F. J. Arregui, I. R. Matias, F. Baldini, *ACS Sensors* **2018**, *3*, 936.
[41] F. Chiavaioli, D. Santano Rivero, I. Del Villar, A. B. Socorro-Leránoz, X. Zhang, K. Li, E. Santamaría, J. Fernández-Irigoyen, F. Baldini, D. L. Van den Hove, L. Shi, W. Bi, T. Guo, A. Giannetti, I. R. Matias, *Adv. Photonics Res.* **2022**, *3*, 2200044.
[42] G. Moro, F. Chiavaioli, S. Liberi, P. Zubiate, I. Del Villar, A. Angelini, K. De Wael, F. Baldini, L. M. Moretto, A. Giannetti, *Results Opt.* **2021**, *5*, 100123.
[43] A. Novikova, A. Katiyi, A. Halstuch, A. Karabchevsky, *Nanomaterials* **2022**, *12*, 2915.
[44] B. Sun, F. Morozko, P. S. Salter, S. Moser, Z. Pong, R. B. Patel, I. A. Walmsley, M. Wang, A. Hazan, N. Barré, A. Jesacher, J. Fells, C. He, A. Katiyi, Z.-N. Tian, A. Karabchevsky, M. J. Booth, *Light: Sci. Appl.* **2022**, *11*, 214.
[45] A. Leal-Junior, L. Avellar, V. Biazi, M. S. Soares, A. Frizera, C. Marques, *Opto-Electron. Adv.* **2022**, *5*, 210098.
[46] A. Karabchevsky, A. Katiyi, M. I. M. Bin Abdul Khudus, A. V. Kavokin, *ACS Photonics* **2018**, *5*, 2200.
[47] J. Zhou, D. Al Husseini, J. Li, Z. Lin, S. Sukhishvili, G. L. Coté, R. Gutierrez-Osuna, P. T. Lin, *Sci. Rep.* **2022**, *12*, 5572.
[48] J. Han, X. Wu, X. Ge, Y. Xie, G. Song, L. Liu, Y. Yi, *Polymers* **2022**, *14*, 3967.
[49] H. Krauss, K. Takemura, *IEEE/ASME Transactions on Mechatronics* **2022**, *27*, 2151.
[50] J. Li, M. Zhang, *Light: Sci. Appl.* **2022**, *11*, 128.
[51] W. Yang, Y. Ma, H. Sun, C. Huang, X. Shen, *TrAC, Trends Anal. Chem.* **2022**, *152*, 116608.
[52] K. Saitoh, S. Matsuo, *Nanophotonics* **2013**, *2*, 441.
[53] B. Da Lio, D. Bacco, D. Cozzolino, N. Biagi, T. N. Arge, E. Larsen, K. Rottwitt, Y. Ding, A. Zavatta, L. K. Oxenløwe, *IEEE J. Sel. Top. Quantum Electron.* **2019**, *26*, 1.
[54] B. Zhu, T. F. Taunay, M. F. Yan, M. Fishteyn, G. Oulundsen, D. Vaidya, *IEEE Photonics Technol. Lett.* **2010**, *22*, 1647.
[55] M. Morant, A. Trinidad, E. Tangdiongga, T. Koonen, R. Llorente, *IEEE Trans. Microwave Theory Tech.* **2019**, *67*, 2928.
[56] A. Klenke, C. Jauregui, A. Steinkopff, C. Aleshire, J. Limpert, *Prog. Quantum Electron.* **2022**, 100412.
[57] E. Bochove, P. Cheo, G. King, *Opt. Lett.* **2003**, *28*, 1200.
[58] C. Jollivet, A. Mafi, D. Flamm, M. Duparré, K. Schuster, S. Grimm, A. Schülzgen, *Opt. Express* **2014**, *22*, 30377.
[59] M. Babaeian, D. T. Nguyen, V. Demir, M. Akbulut, P.-A. Blanche, Y. Kaneda, S. Guha, M. A. Neifeld, N. Peyghambarian, *Nat. Commun.* **2019**, *10*, 3516.
[60] C. Clear, S. A. White, A. Scaroni, et al. **2016**.
[61] R. J. Gagné, *Proc. Entomol. Soc. Wash.* **2016**, *118*, 27.
[62] N. Yoshimi, S. Sugie, H. Iwata, K. Niwa, H. Mori, C. Hashida, H. Shimizu, *Mutation Res./Genetic Toxicology* **1988**, *206*, 183.
[63] M. V. Kulkarni, A. K. Viswanath, P. Khanna, *J. Appl. Polym. Sci.* **2006**, *99*, 812.
[64] S. Shaji, S. M. Eappen, T. Rasheed, K. Nair, *Spectrochim. Acta, Part A* **2004**, *60*, 351.